COBEM 2023 27TH INTERNATIONAL CONGRESS OF MECHANICAL ENGENEERING

ABCM Brazilian Society of Mechanical Sciences and Engineering
27th ABCM International Congress of Mechanical Engineering
December 04-08, 2023, Florianópolis-SC, Brazil

COB-2023-1945
MULTI-OBJECTIVE SHAPE OPTIMIZATION OF A PASSIVE MICROMIXER USING GENETIC ALGORITHM AND MULTI-OBJECTIVE DECISION-MAKING ALGORITHMS

Eduardo Henrique Taube Cunegatto
Kristian Nascimento Telöken
Lenon Audibert Cisco
Flávia Schwarz Franceschini Zinani
Sandro José Rigo
Applied Computing Graduate Program, Universidade do Vale do Rio dos Sinos (UNISINOS). São Leopoldo, RS, Brazil.
Mechanical Engineering Graduate Program, Universidade do Vale do Rio dos Sinos (UNISINOS). São Leopoldo, RS, Brazil.
eduardohtc@edu.unisinos.br
kteloken@edu.unisinos.br
lenonac@edu.unisinos.br
fzinani@unisinos.br
rigo@unisinos.br

Abstract. *In this work, the Constructal Design Method (CDM), based on the Constructal Law, combined NSGA-II algorithm, is used to optimize the shape of a micromixer, with five degrees of freedom, in terms of mixing percentage and pressure drop for a Peclet number of 500. The systems are modeled by Computational Fluid Dynamics (CFD) solutions, using Navier-Stokes and species equations to predict the flow and mixing of water-dye mixture. The simulations were designed via Central Composite design method, and the results were used to create second-order metamodels for mixing percentage and pressure drop, employed in the multi-objective optimization via NSGA-II algorithm. With the best set of solutions (Pareto curve) defined, the multi-criteria decision-making algorithms (LINMAP, TOPSIS, and VIKOR) were employed. The results showed that the shape with the highest mixing percentage also has the highest pressure drop. Using the decision methods to choose an optimized solution, it was possible to find shapes that returned a mixing percentage of 12.2%, 18.3%, and 4.9% lower than the maximum, but with 50.2%, 64.7%, and 23.7% fewer pressure drops, respectively. The approach combining statistical, numerical, and optimization to CDM allowed the finding of the best geometric design, which is mandatory for passive micromixers.*

Keywords: *Multi-objective optimization, Passive micromixer, Constructal Design, CFD, Genetic Algorithms*

1. INTRODUCTION

In recent years, the miniaturization of devices has played a crucial role in developing advanced technologies in various fields such as chemistry, biology, engineering materials and medicine. Due to the compact size of those devices, many application opportunities are emerging, such as pathogen detection in food (Lonchamps et al., 2022), microfluidic sensors (Li et al., 2022), and organ-on-a-chip (Saorin et al., 2022). Among these devices, micromixers have gained prominence as fundamental components for conducting chemical mixing on a small scale (Gopi, et al., 2022).

Many applications can be found for those devices, such as diagnosing diseases and producing pharmaceuticals and new materials (Li et al., 2022). Also, microchips coupled with micromixers are used in many applications. One of the most important nowadays is the lab-on-a-chip (LOC) device, which conducts laboratory functions on a miniaturized scale. Another example is the organ-on-a-chip (OOC), which combines biological and microtechnological aspects to reproduce aspects of human physiology via microchannels that guide and manipulate solutions (Leung et al., 2022).

Micromixers can be separated into two distinct mixing mechanisms: active and passive. The first uses external forces, such as electromagnetic fields, sound waves, electric fields, or heat transfer, while the second uses only geometrical features to enhance the mixing (Li et al., 2022). Thus, the efficiency of a micromixer is largely determined by its geometric design, which directly influences the mixing rate and the quality of chemical reactions occurring within the device. However, seeking the optimal design of a micromixer is a complex challenge as multiple design criteria must be simultaneously considered.

Many works in the literature present micromixers optimization with many proposed designs. Works from Wang et al. (2012), Rahmannezhad and Mirbozorgi (2019), Mainochi et al. (2022) and Antognoli et al. (2023) used Y-shaped passive micromixers with round obstacles in the main channel to enhance the mixture and evaluated the using numerical analysis. Also, the use of fractal-like shapes to design the micromixer can be found in the works of Zhang et al. (2019), Chen et al. (2020) and Chen and Lv (2022), which proved to be an optimal way to enhance the mixing performance. Also,

innovative shapes such as presented by Kouadri et al. (2021) and Santana et al (2022) bring different split and recombine designs.

In this context, searching for design techniques becomes essential in finding efficient solutions in the design space. One technique which is relatively new but with crescent use is Constructal Design method. This method is based on Constructal Theory established by Bejan (1997), and further explained and explored by Bejan and Lorente (2008) and its basis relies upon the laws of evolution found in nature, in which living systems evolve their configurations to facilitate access to the flows that keep them alive. This method can be found applied in micromixer design in the works of Borahel et al. (2022), Cunegatto, et al. (2023a), Cetkin and Miguel (2019) and Cunegatto et al. (2023b).

Along with the design technique, an optimization technique must also be employed. For multi-objective optimization, genetic algorithms are prevalent, particularly the NSGA-II. The efficiency of this algorithm is demonstrated in works such as Liu et al. (2023), Sui et al. (2022), Deng et al. (2020), Wang et al. (2022) and Nikpour and Mohebbi (2022), the last being applied in micromixer design. These works also employed multi-criteria decision-making algorithms (MCDMa) such as LINMAP, TOPSIS and VIKOR, to assist in selecting the best solution based on preferences and weightings of different criteria involved.

Therefore, this work aims to apply Constructal Design method, NSGA-II algorithm in conjunction with multicriteria decision algorithms to optimize the shape of a micromixer. Criteria such as mixing efficiency and pressure drop will be considered. Constructal Design method is used to the problem design and NSGA-II will be employed to find a set of optimal solutions in terms of these criteria. At the same time, multicriteria decision algorithms will assist in selecting the best solution to meet specific project requirements. It is expected that the results of this work will contribute to the development of more efficient and customized micromixers by combining the perspectives of Constructal Design, mixing-pressure drop multi-objective optimization and different decision-making methods.

2. METHODOLOGY

2.1 Constructal Design

The application of the Constructal Design method is based on a step-by-step scheme, first introduced by Rocha et al. (2017) and recently improved by Cunegatto et al. (2023a). Overall, this method presupposes the definition of a finite-size system, identifying what is flowing in the system, that is, what will cause a better performance on the system when it is enhanced, the very performance indicator(s), the definition of constraints and degrees of freedom and methods of experimentation/simulation and evaluation of the system's performance.

Step 1: System Definition

The system under analysis in this work is a passive micromixer. Two distinct species enter the device via two separate inlets and flow in the direction of the outlet, as shown in Figure 1. The micromixer can be divided into two main sections: the Y-shaped inlets and the channel. Both species enter the device at the same speed at each inlet. The mixing process occurs in the mixing channel, which is 10 mm long and 200 μm wide. Rectangular-like obstacles (18 in total), with a length of 400 μm, are placed along the channel length to improve the mixing performance. While their length remains constant, their height is varied in 5 different sections to alter their shape. The center of each obstacle is separated by 500 μm.

Step 2: Identifying what is flowing

It is redundant to say that two different fluid species are flowing in the system. However, this step is related to the Constructal Design method's perspective considering the purpose of the flow. Thus, the system aims to promote the mixing between species that flows through the channel, so what is being facilitated and/or enhanced is the advective-diffuse flow of mixing species.

Step 3: Performance indicator

In this study, we have two performance indicators: mixing percentage (φ) and pressure drop (ΔP). The mixing percentage is measured by the concentration profile in a vertical section of the main channel, which is the outlet section in our case. Mathematically, the mixing percentage is expressed by:

$$\varphi = \left(1 - \frac{\sigma}{\sigma_{max}}\right) \cdot 100\ [\%_{mix}] \tag{1}$$

where σ represents the standard deviation and the subscript *max* indicates the maximum standard deviation, which is 0.5 for a mixture of two species. The expression used to calculate the standard deviation is:

$$\sigma = \sqrt{\frac{1}{N-1}\sum_{j=1}^{N}\left(C_j - \overline{C}_j\right)^2} \tag{2}$$

where N is the number of sample points in the vertical section, C_j is one species concentration in a j point, and $\overline{C_j}$ is the average value of the concentration of that species in that section:

$$\overline{C_j} = \frac{\sum_{j=1}^{N} C_j}{N} \tag{3}$$

As for the pressure drop, it is the difference between the inlet and outlet pressure, which is also measured in the vertical section of those boundaries. Mathematically, it can be expressed as:

$$\Delta P = P_{inlet} - P_{outlet} \tag{4}$$

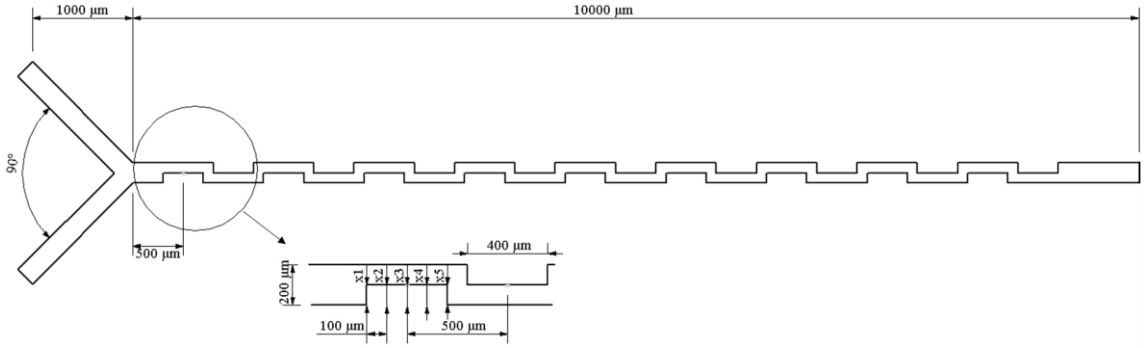

Figure 1. Schematic of the physical system.

Step 4: Constraints

Constraints can be interpreted as geometric parameters and features that are not modified and remained constant. So, aside from the height of the obstacles, all the dimensions and parameters shown in Figure 1 are the constraints of the system.

Step 5. Degrees of freedom

In the opposite way of the constraints, degrees of freedom are the geometric parameters and features that are changed during the system evaluation. In this study, we propose to modify the shape of the obstacles, in five different sections, by changing the height of each section. As shown by the detailed schematic in Figure 1, each section is represented as x_n, and they have equal lengths. So, the system has five degrees of freedom, which is summarized as:

$0.020 < x_1, x_2, x_3, x_4, x_5 < 0.100$ [µm]

Step 6. Method of Experimentation/Simulation

To evaluate the mixing percentage and pressure drop, computational fluid dynamics (CFD) is used, via ANSYS Fluent 2022R2 software (ANSYS, 2022), which is based on the Finite Volume Method (Patankar, 1980). To determine which configuration is simulated, a Central Composite Design (CCD) method (Montgomery, 2012), was employed, using the *R Statistic* programming language. For a five-degree-of-freedom system, a CCD run takes 43 simulations, which are used to create the database for the optimization process.

Once all the CCD simulations are done, the mixing percentage and pressure drop results are gathered to create the dataset. With it, **a second order polynomial model is created for each variable (φ and ΔP)**, described by Equation 5, which can be used to predict the response inside the design space.

$$(\varphi, \Delta P) = \beta_0 + \sum_{i=1}^{5} \beta_i x_i + \sum_{i=1}^{5} \beta_{ii} x_i^2 + \sum_{i \neq j}^{5} \beta_{ij} x_i x_j \tag{5}$$

where x represents the independent variables, φ and ΔP the response variables and β the regression coefficients.

Before proceeding to the next step, the model's fit and precision are evaluated to verify if more data is necessary to build a high-fidelity model. This is done by analyzing the Mean Absolute Error (*MAE*) and Coefficient of Determination (R^2). The first represents the absolute difference between the predicted and simulated results, while the second represents how well the model fits the simulated results (El Hami and Pougnet, 2020). A satisfactory model is achieved when both *MAE* is less than 1% of the maximum value and R^2 is higher than 90% (Cunegatto et al., 2022). They are mathematically represented by equations 6 and 7 respectively,

$$MAE = \frac{\sum_{i=1}^{m} |(\varphi, \Delta P)_{pred_i} - (\varphi, \Delta P)_{sim_i}|}{m} \tag{6}$$

$$R^2 = 1 - \frac{\sum_{i=1}^{m} \left((\varphi, \Delta P)_{sim_i} - (\varphi, \Delta P)_{pred_i}\right)^2}{\sum_{i=1}^{m} \left((\varphi, \Delta P)_{sim_i} - \overline{(\varphi, \Delta P)_{sim_i}}\right)^2} \tag{7}$$

where the subscripts *pred* and *sim* represent the values predicted by the model and the ones obtained in the simulations, respectively; *m* represents the number of simulation data used to build the model; the bar in the denominator of Equation 7 represents the mean value of the variable.

Step 7. Evaluation of the System

As both models are adequate, the next step is the optimization process. Among the optimization tools, the Genetic algorithm (GA) has been a popular choice, and its foundation lies in genetic principles and natural evolution found in nature. For a multi-objective purpose, Deb et al. (2002) proposed the NSGA-II (Non-Sorted Genetic Algorithm), which is still used to this day.

The overall steps of the optimization process are presented in Figure 2, which is based on the work of Wang et al. (2022), but can be summarized in 4 key steps:

1. A random initial population of solutions is generated inside the design space.
2. This initial population is then evaluated, through the mathematical model, based on the objectives of the problem, which are, in our case, the **maximization of the mixing percentage** and the **minimization of the pressure drop**. This evaluation leads to a classification, which separates the dominant and non-dominated solutions.
3. Non-dominated solutions are bound to selection, crossover, and mutation operations to generate a new population of solutions.
4. The current population is combined with the new generated population and a new evaluation is performed. Once the termination criterium is achieved, that is, the number of generations, a final set of solutions is obtained, known as the Pareto optimal solutions.

Since the multi-objective optimization process leads to a set of solutions, and each solution offers a tradeoff between the objective variables, decision-making algorithms play an important role to help to find the best solution for the problem. The selected algorithms for this purpose are LINMAP (Linear Programming Technique for Multidimensional Analysis of Preference), TOPSIS (Technique for Order Preference by Similarity to Ideal Solution), and VIKOR (Visekriterijumska Optimizacija I Kompromisno Resenje) or Multicriteria Optimization and Compromise Solution (Opricovic and Tzeng, 2004).

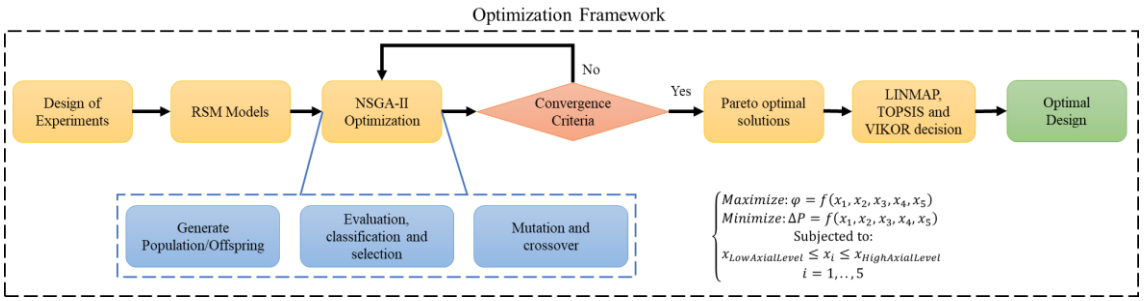

Figure 2. The framework of the optimization process.

The LINMAP method is very simple, and it considers only the ideal solution. Thus, the selected solution is the one whose Euclidian distance (Equation 8) to the ideal solution is the shortest:

$$d_L = \sqrt{\sum_{j}^{2} (k_{ij} - O_j)^2}, i = 1,2,..,n \tag{8}$$

where d_L represents the selected solution, *k* represents a single solution, *O* represents the ideal solution and *n* represents the number of Pareto optimal solutions.

The TOPSIS method is very similar, but it also considers the non-ideal solution as well. It also requires the assignment of weights for each objective variable. Then, the Euclidean distance between the ideal and non-ideal solutions is calculated using equations 9 and 10:

$$(d_i^+, d_i^-) = \sqrt{\sum_j^2 (w_j(k_{ij} - (O_j^+, O_j^-)))^2} \ , i = 1,2,..,n \tag{9}$$

where the superscripts + and – represents ideal and non-ideal references and *w* represents the weight. In this work, **weights of 0.7 and 0.3** are assigned to φ and ΔP, respectively. The final step is to calculate the closeness *C* of each solution to the ideal solution, which is done using Equation 11, whose solution with the shortest distance is selected:

$$C_i = \frac{d_i^-}{d_i^- + d_i^+} \ , i = 1,2,\dots,n \tag{10}$$

The VIKOR method has a more complex approach since it requires more calculations before reaching a result. For this paper, the method is summarized in the steps shown below, but we recommend Opricovic and Tseng (2004) paper for an in-depth analysis of the methodology. It's important to note that this method also uses weights for each objective variable, which, in our case, are the same as proposed in the TOPSIS method. The main steps for the VIKOR method are:

- **Normalization and weighting**: the values of the database are normalized to reach the same scale. Then, the weights are assigned based to each objective variable, based on its importance.
- **Ideal and non-ideal solutions**: this step shares the same idea as TOPSIS. From the normalized values, two reference solutions, ideal (best solution of each criterion) and non-ideal (worst solution of each criterion).
- **Calculation S and R distances**: for each solution, both normalized and weighted S_i and R_i distances are calculated, considering the ideal and non-ideal solutions.

$$S_j = \sum_j^2 \frac{w_j(O_j^+ - x_{ij})}{(O_j^+ - O_j^-)} \tag{11}$$

$$R_j = \max\left[\frac{w_j(O_j^+ - x_{ij})}{(O_j^+ - O_j^-)}\right] \tag{12}$$

- **Calculate the Q metric:** this metric considers the previous distances and is the final key to finding the best solution. It is mathematically expressed by Equation 13:

$$Q_j = \frac{v(S_j - \min(S_j))}{(\max(S_j) - \min(S_j))} + \frac{(1-v)(R_j - \min(R_j))}{(\max(R_j) - \min(R_j))} \tag{13}$$

where *v* is the 'maximum group utility weight', which is equal to 0.5.

- **Q classification:** the results are classified in decreasing order by their *Q* value. The solution with the lowest *Q* is the chosen one.

2.2 Mathematical modeling

The problem of mixing fluids, in a two-dimensional domain, is modeled by the steady-state equations of mass, momentum, and species balance for incompressible Newtonian fluids. These equations are described, respectively, as:

$$\frac{\partial u}{\partial x} + \frac{\partial v}{\partial y} = 0 \tag{14}$$

$$\rho\left(u\frac{\partial(u,v)}{\partial x} + v\frac{\partial(u,v)}{\partial y}\right) = -\frac{\partial P}{\partial(x,y)} + \mu\nabla^2(u,v) \tag{15}$$

$$\left(u\frac{\partial C_1}{dx} + v\frac{\partial C_1}{\partial y}\right) = D_{12}\nabla^2 C_1 \tag{16}$$

where u and v are the velocity vector components in directions x and y respectively, P is the pressure, ρ is the mixture density, μ is the mixture viscosity, C_1 is the molar concentration of species 1, D_{12} is the mass diffusion coefficient ($1e^{-9}$) and ∇^2 is the tensorial relation.

Considering that two distinct fluids, water, and dyed water, enter the domain, with velocities equal to V_{in} and concentrations C_1 equal to 1 and 0, respectively, the mixture properties, density, and viscosity are calculated by Equations 17 and 18:

$$\rho = \frac{1}{\frac{C_1}{\rho_w} + \frac{C_2}{\rho_{dw}}} \tag{17}$$

$$\mu = C_1\mu_w + C_2\mu_{dw} \tag{18}$$

where the subscripts w and dw refers to water and dyed water, whose density is 998.2 kg/m³ and viscosity is $8.9e^{-4}$ Pa.s, for both fluids (Rahmannezhad and Mirbozorgi, 2019).

The Reynolds and mass Peclet numbers for this problem are given by:

$$Re = \frac{\rho W V_{in}}{\mu} \tag{19}$$

$$Pe = \frac{W V_{in}}{D_{12}} \tag{20}$$

where W is the main channel width, 200 μm. For this problem, we are considering Pe = 500, which is a typical value found in the literature in the works of Santana et al. (2021), Nikpour and Mohebbi (2019) and Kouadri et al. (2021) for example.

2.3 Numerical modeling

As mentioned in the previous section, the ANSYS Fluent 2022R2 was employed to solve the equations. The pressure-velocity scheme COUPLED was used, along with PRESTO (Pressure Staggering Option) for Pressure interpolation, QUICK (Quadratic Upstream Interpolation for Convective Kinematics) for momentum, and Third Order MUSCL (Monotonic Upstream-centered Scheme for Conservation Laws) for species equation. The convergence criteria for mass, momentum, and species were 10^{-6}, $10^{-8,}$ and 10^{-7}, respectively. This configuration set was based on the results of the works from Ortega-Casanova (2017) and Kouadri et al. (2021), which showed high fidelity using these configurations when compared to experimental data.

For the boundary conditions, both fluids enter the domain with a prescribed velocity V_{in}, while the concentration C_1 is 1 for the upper inlet and 0 for the lower. At the outlet, a gauge pressure of 0 Pa is considered, and the walls are assumed to be no slip and impermeable. The model, as well as the mesh employed in this study, was validated by the authors in Cunegatto et al. (2023b). Figure 3 shows the boundary conditions schematic.

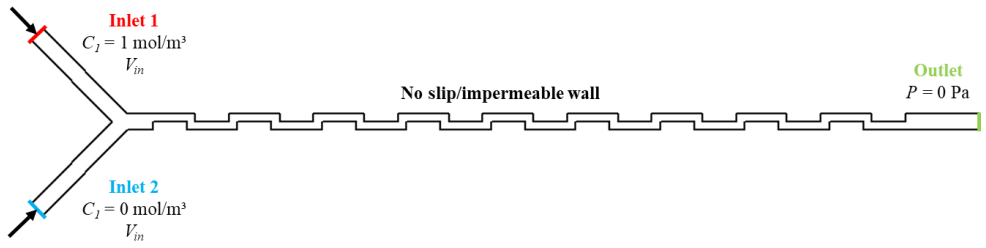

Figure 3. Schematic of the boundary conditions.

3. RESULTS

From the 43 simulations generated by the Central Composite Design, two mathematical models, one for each objective variable (φ and ΔP) were created. Then, they were evaluated by the metrics R^2 and MAE to see if the required criteria are met. To help the visualization of those metrics, Figure 4 shows the fit plots for each model, as well as their values.

In the graphs shown in Figure 4, the red dots represent the values predicted by the model, while the line represents the true (simulated) values. For both models, the dots are aligned with the line, which is a good indicator of precision, and

the metrics confirm that. R^2 means how much the model can predict the variation of the objective variable, so, in this case, over 99% of the variation can be predicted by the models, which means that, for any given configuration inside the design space, the model will predict with a high level of confidence.

As for *MAE*, it can be interpreted as the distance between the points and the line. That is, the closer the points are to the line, the lower is *MAE*. So, as mentioned in the previous paragraph, along with the high variation being predicted by the model, it also may predict values with a maximum tolerance indicated by ± *MAE*. Even with similar values of R^2, the *MAE* for Pressure drop is higher. This happens because the range of values is higher, thus, the data has more variation, which causes the model to find the right adjustment, in trade of precision. However, since the metrics satisfy the criteria, both models are adequate.

The evaluation of those metrics is critical because, during the application of the NSGA-II algorithm, many configurations will be tested and used to build the final solutions. So, since the models were adequate to feed the NSGA-II, the setup for it was defined as: a maximum number of generations of 175, a population size of 125, a crossover probability of 0.9, and a mutation rate of 0.1. After 175 generations, the final Pareto curve shows 123 possible solutions for the problem, which are shown in Figure 5, along with the decision-making algorithms solutions and the shapes.

Each point in the Pareto optimal solutions (Pareto front) represents a non-dominated solution, meaning that, at least, one of the objectives is better than another. So, each solution along the curve will be better than the other in one aspect, either maximizing φ or minimizing ΔP. That's when decision-making algorithms become essential.

As for the TOPSIS solution, which considers both ideal and non-ideal solutions, the chosen solution returns a value of 60.76% for mixture percentage and around 40.13 Pa. This value is far from com the maximum mixing (74.37%) but is not that far from the minimum pressure (around 28 Pa). Considering the weights employed in this methodology, the expected mixture was quite low, which is closer to the minimum mixing value.

Regarding LINMAP, the chosen solution is around the middle range of the mixing percentage, with a value of 65.22%, and a pressure drop of 59.39 Pa. This solution only considers the optimal value and offers a tradeoff of increasing the pressure drop to increase the mixture percentage, compared to the previous one.

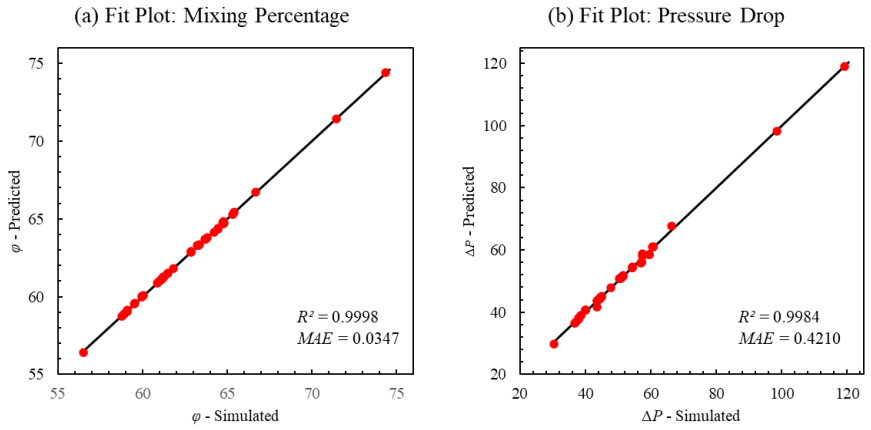

Figure 4. Fit plots of the models: (a) Mixing percentage and (b) Pressure drop.

Finally, for the VIKOR solution, it responds better to the weights. That is, the mixing percentage is 70.95%, the closest to the maximum among the chosen solutions, but also has the highest pressure drop, of around 90.66 Pa. As it was defined, the maximization of the mixing percentage has more value than the minimization of the pressure drops. Thus, it was expected a solution that yields a high mixing, without harnessing considerably the pressure drop.

From the geometric evolution graph in Figure 5, the maximum mixing design is the original shape, with their values at maximum height (0.1 mm), which is also the maximum area occupied by a single obstacle. So, to reduce the pressure drop, but to keep a high mixing percentage, the VIKOR solution "sculpted" the max solution by removing a few zones by reducing the height (points 1 and 3), and keeping points 2,4, and 5 at maximum height.

LINMAP solution cuts even more the shape, and, by analyzing the values from the table, it provided a significant reduction in the pressure drop. Also, point 4 remained the highest for this design, being slightly smaller than the previous one. Point 3, also has a shorter value, being a shape feature that is related to the balance between maximizing mixing percentage and minimizing pressure drop. The TOPSIS solution, however, returned with a rectangular shape.

Comparing the three solutions, it is possible to notice a few connections between them. From VIKOR to LINMAP, it is possible to notice that point 3 acts like a "hole" and point 4 is the highest, being a zone that might cause a high detour on the flow. As for LINMAP and TOPSIS, not much can be related aside from the identical heights at point 5 and the flat region between points 1 and 2.

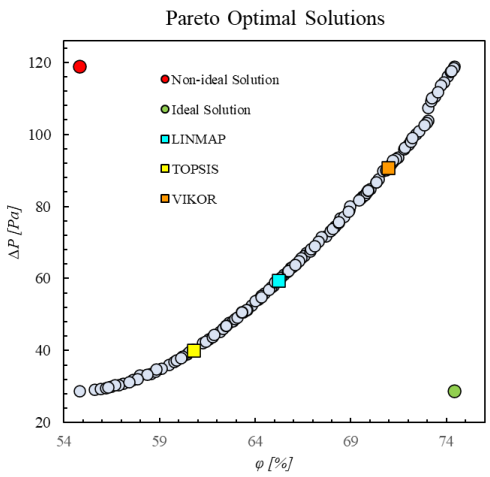

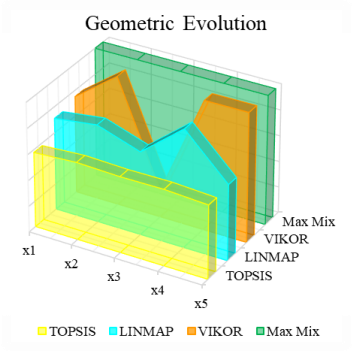

Table of Solutions

x_1	x_2	x_3	x_4	x_5	φ_{NSGA}	ΔP_{NSGA}	φ_{CFD}	ΔP_{CFD}		φ Diff from max	ΔP Diff from max
0.100	0.100	0.100	0.100	0.100	74.394	118.961	74.370	119.149	Max Mix	-	-
0.075	0.100	0.021	0.100	0.100	70.950	90.664	70.719	90.934	VIKOR	-4.91%	-23.68%
0.071	0.075	0.064	0.091	0.059	65.218	59.397	65.293	59.360	LINMAP	-12.21%	-50.18%
0.058	0.060	0.059	0.059	0.057	60.765	40.126	60.758	42.075	TOPSIS	-18.30%	-64.69%

*Values in mm

Figure 5. Pareto optimal solutions with the selected solutions from the decision-making algorithms.

Also, the table shows the compared values between the ones predicted by NSGA and CFD simulations. The values are close to each other, except for the pressure drop from the TOPSIS solution, which was underestimated by the model. Still, this difference does not compromise the model at all because it is still below 5%, which is considerable. Otherwise, all the optimization processes would have to be repeated, which is not a good tradeoff, since the other results are adequate. Lastly, the differences between the mixing percentage between the designs show that, from the weights used in this work, it was possible to tradeoff above 20% of pressure drop and reduce 5% (for VIKOR solution) or a higher tradeoff of 65% for 18% (TOPSIS solution). This emphasizes that the set of weights is a very important factor in multi-objective optimization.

Figure 6 shows the concentration and pressure contours along the main channel of each solution. The left side of the concentration contours represents the inlet section of the channel, near the region where the fluids enter in contact with each other. The central "line", in green, represents the concentration boundary layer and is very thin at the beginning, and is covered with pure species (water and dyed water). Upon reaching the obstacles, the mixing process starts to increase, as the boundary layers get thicker as they pass through the obstacles. At the outlet, it can be observed that there are no pure species, only mixed ones, with different intensities, around a 70/30 ratio, based on the color bar.

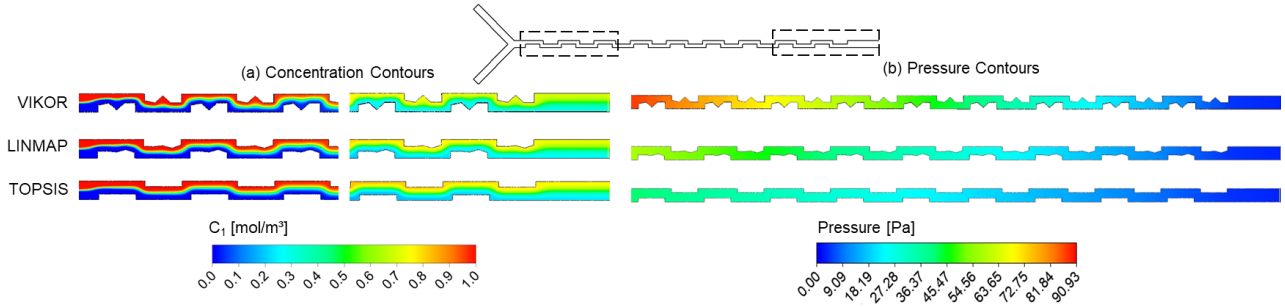

Figure 6. (a) Concentration and (b) Pressure contours for VIKOR, LINMAP, and TOPSIS solutions.

Overall, all the designs provide mechanisms to enhance such as the reduction of the diffusion path with the obstacles, meaning that the obstacle height reduces the channel width, so the boundary layer of each fluid is closer to each other. Not only the reduction of diffusion path, but the obstacles also cause the flow to change direction, which enhances mass diffusion as one fluid goes to the direction of the other; and the higher the obstacle, the greater those effects.

Based on the previous appointments, the VIKOR solution is the one that provides the best mixing-enhancing performance, as previously seen by the results in Figure 5. The increased height of the shape provides a great reduction in the mixture path. Also, one peculiar characteristic is the "V" shape in the middle of the obstacle; the sudden reduction in the height of the obstacle also changes the flow direction. LINMAP solution also allows for the flow to change its path as they pass through it. As for the TOPSIS solution, the flat solution does not enhance mass diffusion, making it slower than the other solutions. However, as seen in the pressure drop contours, the VIKOR has a more significant tradeoff

compared to the other solutions, as the pressure required for the mixture to pass each obstacle is much higher. Still, it's important to reiterate that this tradeoff was expected by the weights assigned to each objective variable.

4. CONCLUSION

This study performed a multi-objective shape optimization of a passive micromixer based on the principles of the Constructal Design method and Genetic Algorithm. CDM was used as guidance to build the optimization setup, from the initial configuration to the mathematical model. From the model, GA was applied to find a set of solutions aiming to maximize the mixing percentage and minimize the pressure drop from the micromixer. Three multi-objective decision-making algorithms, VIKOR, TOPSIS, and LINMAP, were employed to choose the best solution from the set.

LINMAP solution only considers the best possible solution. In contrast, the others consider the best and worst solution, and weights for each variable. Those weights greatly influence the result and should be chosen based on the importance of each objective variable in the problem.

Each result from the decision-making algorithms was compared with a solution that achieved the maximum mixing, inside the design space. It was possible to obtain solutions with 23%, 50%, and 64% less pressure drops with 5%, 12%, and 18% less mixing percentages with VIKOR, LINMAP, and TOPSIS, respectively. From this, it was seen that, depending on the weights, this difference will change towards one objective or another, and each method will respond differently to it. VIKOR method seemed to respond better to the weights, while TOPSIS has more impact from the ideal and non-ideal solutions; and LINMAP offers a balance between the two, considering only the ideal solution, being a good algorithm to be employed, specifically when comparing to other solutions. The shapes provided by each solution were analyzed and each one provides different ways to improve mass transfer, specially VIKOR and LINMAP. Their peculiar shape not only provided a reduction in the diffusion path, by reducing the channel width but also provided means for the flow to change its direction while it passes through the obstacles, enhancing even more the mixing percentage.

With the advancement of Constructal Design method and multi-objective optimization techniques, the applied methodology brings an innovative and versatile approach towards development of efficient devices, especially in microfluidics. For future projects, it is possible to increase the degrees of freedom of the system and test the current design under different flow conditions.

5. ACKNOWLEDGEMENTS

This work was funded by CAPES, CNPq and FAPERGS. E.H.T. Cunegatto, K.N. Telöken and L.A. Cisco are CAPES scholarship holders (Code 001). F. Zinani is a grant holder of CNPq (Proc. No. 311444/2021-0). The project was funded by FAPERGS via the PqG public notice (Proc. No. 21/2551-0002169-1).

6. REFERENCES

Ansys® Fluent, Release 2022 R2, Help System, Ansys Fluent Theory Guide, ANSYS, Inc.

Antognoli, M.; Donato, L.; Galleti, C.; Stoecklein, D.; Di Carlo, D.; Brunazzi, E. Pre-arranged sequences of micropillars for passive mixing control of water and ethanol, Chemical Engineering Journal, v. 461, p. 141851, 2023.

Bejan, A. Constructal-theory network of conducting paths for cooling a heat generating volume. International Journal of Heat Mass Transfer, v. 40, 799-816, 1997.

Bejan, A; Lorente, S. Design with Constructal Theory, John Wiley & Sons, Inc, New Jersey, 2008.

Borahel, R.S.; Zinani, F.S.F.; Rocha, L.A.O.; Dos Santos, E.D.; Isoldi, L.A.; Biserni, C. Geometric optimization of a rectangular isothermal block inside a lid-driven cavity by means of constructal design. International Communications in Heat and Mass Transfer, v. 139, 2022.

Cetkin, E.; Miguel, A.F. Constructal branched micromixers with enhanced mixing efficiency: Slender design, sphere mixing chamber and obstacles. International Journal of Heat and Mass Transfer, v. 131, 2019.

Chen, X; Lv, H. New insights into the micromixer with Cantor fractal obstacles through genetic algorithm. Sci Rep 12, 4162 (2022).

Chen, Y.; Chen, X.; Liu, S. Numerical and experimental investigations of novel passive micromixers with fractal-like tree structures, Chemical Physics Letters, v. 747, p. 137330, 2020.

Cunegatto, E.H.T.; Gotardo, M.; Zinani, F.S.F. Constructal Design and Response Surface modeling of tube arrangement heat exchanger with two degrees of freedom for pseudoplastic and viscoplastic fluids. In: 19th Brazilian Congress of Thermal Sciences and Engineering, 2022, Bento Gonçalves, RS. Fluid Mechanics and Rheology: Rheology and Non-Newtonian Fluid Mechanics, 2022. DOI: http://dx.doi.org/10.26678/ABCM.ENCIT2022.CIT22-0082

Cunegatto, E.H.T.; Gotardo, M; Zinani, F.S.F. Numerical analysis of tube arrangements with one, two, and four degrees of freedom for heat transfer with pseudoplastic fluids. International Journal of Heat and Mass Transfer, v. 208, p. 124080, 2023. a.

Cunegatto, E.H.T.; Zinani, F.S.F.; Biserni, C.; Rocha L.A.O. Evolutionary Design of Passive Micromixers with Multiple Obstacles Via Computational Fluid Dynamics. International Journal of Heat and Mass Transfer, v. 215, p. 124519, 2023. b.

Deb, K.; Pratap, A.; Agarwal, S.; Meyarivan, T. A fast and elitist multiobjective genetic algorithm: NSGA-II, in IEEE Transactions on Evolutionary Computation, vol. 6, no. 2, pp. 182-197, April 2002, DOI: 10.1109/4235.996017.

Deng, Y.; Yu, B.; Sun, D. Multi-objective optimization of guide vanes for axial flow cyclone using CFD, SVM, and NSGA II algorithm, Powder Technology, v. 373, p. 637-646, 2020.

El Hami, A.; Pougnet, P. Embedded Mechatronic Systems 2. Elsevier, 2015.

Gopi, R.; Thangarasu, V.; M.V, Angkayarkan.; Ramanathan, A. A critical review of recent advancements in continuous flow reactors and prominent integrated microreactors for biodiesel production, Renewable and Sustainable Energy Reviews, v. 154, p. 111869, 2022.

Kouadri, A.; Douroum, E.; Lasbet, Y.; Nass, T.T.; Khelladi, S.; Makhlouf, M. Comparative study of mixing behaviors using non-Newtonian fluid flows in passive micromixers. International Journal of Mechanical Sciences, v. 201, 2021.

Leung, C.M.; De Haan, P.; Ronaldson-Bouchard, K. et al. A guide to the organ-on-a-chip. Nat Rev Methods Primers, v.2, 2022.

Li, Z.; Zhang, B; Dang, D.; Yang, X.; Yang, W.; Liang, W. A review of microfluidic-based mixing methods. Sensors and Actuators A: Physical, v. 344, 2022.

Liu, Z.; Luo, J.; Pan, Y.; Li, J.; Li, L.; Wei, X.; Xu, H.; Tie, Y.; Zhang, C.; Yang, D. Multi-objective optimization of the performance and emission characteristics for a dual-fuel engine with hydrogen addition, Fuel, v. 332, p. 126231, 2023.

Lonchamps, P.L.; He, Y.; Wang, K.; Lu, X. Detection of pathogens in foods using microfluidic “lab-on-chip”: A mini review. Journal of Agriculture and Food Research. v. 10, 2022.

Mainochi, D.O.; Ainsten, L.; Dos Santos, F.P; Junior, M.B.S. Computational fluid dynamics and machine learning as tools for optimization of micromixers geometry. International Journal of Heat and Mass Transfer, v. 194, 2022.

Montgomery, D.C. Design and Analysis of Experiments, 8. Ed., John Wiley & Sons, New Jersey, 2012.

Nikpour, M; Mohebbi, A. Optimization of micromixer with different baffle shapes using CFD, DOE, meta-heuristic algorithms and multi-criteria decision making. Chemical Engineering & Processing: Process Intensification, v. 170, 2022.

Opricovic, S.; Tseng, G. Compromise solution MCDM methods: A comparative analysis of VIKOR and TOPSIS, European Journal of Operational Research, v. 156, p. 445-455, 2004.

Ortega-Casanova, J. Application of CFD on the optimization by response surface methodology of a micromixing unit and its use as a chemical microreactor. Chemical Engineering & Processing: Process Intensification, v. 117, 2017.

Patankar, S. V. Numerical Heat Transfer and Fluid Flow. McGraw-Hill, New York, 1980.

Rahmannezhad.J.; Mirbozorgi, S.A. CFD analysis and RSM-based design optimization of novel grooved micromixers with obstructions, International Journal of Heat and Mass Transfer, v. 140, p. 483-497, 2019.

Rocha, L.A.O; Lorente, S; Bejan, A. Constructal Theory in Heat Transfer. In: Handbook of thermal Science and Engineering. [S.1]: Springer, p. 329 370, 2017.

Rocha, L.A.O.; Lorente, S.; Bejan, A. Constructal theory in heat transfer, in: Kulacki, F.A. (Ed.), Handb, Therm. Sci. Eng, Springer Cham, 2018.

Santana, H.S.; Silva, J.L.; Da Silva, A.G.P.; Rodrigues, A.C.; Amaral, R.L.; Noriler, D.; Taranto, O.P. Development of a New Micromixer “Elis” for Fluid Mixing and Organic Reactions in Millidevices, Ind. Eng. Chem. Res. V. 60, p. 9216-9230, 2021.

Saorin, G.; Caligiuri, I.; Rizzolio, F. Microfluidic organoids-on-a-chip: The future of human models. Seminars in Cell & Developmental Biology. 2022.

Sui, Z.; Sui, Y.; Wu, W. Multi-objective optimization of a microchannel membrane-based absorber with inclined grooves based on CFD and machine learning, Energy, v. 240, p. 122809, 2022.

Wang, G.; Ding, G.; Liu, R.; Xie, D.; Wu, Y.; Miao, X. Multi-objective optimization of a bidirectional-ribbed microchannel based on CFD and NSGA-II genetic algorithm, International Journal of Thermal Sciences, v. 181, p. 107731, 2022.

Wang, L.; Liu, D.; Wang, X.; Han, X. Mixing enhancement of novel passive microfluidic mixers with cylindrical grooves. Chemical Engineering Science, v. 81, 2012.

Zhang, S.; Chen, X.; Wu, Z.; Zheng, Y. Numerical study on stagger Koch fractal baffles micromixer, International Journal of Heat and Mass Transfer, v. 133, p. 1065-1073, 2019.

7. RESPONSIBILITY NOTICE

The authors are the only responsible for the printed material included in this paper.